KeAi

CHINESE ROOTS
GLOBAL IMPACT

Contents lists available at ScienceDirect

Petroleum Science

journal homepage: www.keaipublishing.com/en/journals/petroleum-science



Original Paper

Petroleum recovery from salt cavern through natural gas displacement: Insights from a gas—oil two-phase flow model with gas dissolution and exsolution



You-Qiang Liao ^a, Tong-Tao Wang ^{a,*}, Tao He ^a, Dong-Zhou Xie ^b, Kai Xie ^c, Chun-He Yang ^a

- ^a State Key Laboratory of Geomechanics and Geotechnical Engineering Safety, Institute of Rock and Soil Mechanics, Chinese Academy of Sciences, Wuhan, 430071, Hubei, China
- ^b School of Resources and Environmental Engineering, Wuhan University of Technology, Wuhan, 430070, Hubei, China
- ^c PipeChina Engineering Technology Innovation Co., Ltd, Tianjin, 300450, China

ARTICLE INFO

Article history: Received 12 February 2025 Received in revised form 9 June 2025 Accepted 10 June 2025 Available online 14 June 2025

Edited by Yan-Hua Sun

Keywords:
Petroleum recovery
Natural gas displacement
Feasibility analysis
Salt cavern
Gas-oil two-phase flow
Gas dissolution and exsolution

ABSTRACT

The challenge of wide brine source and its additional problems come from the economy (energy consumption and other costs), security (re-dissolution of surrounding salt rocks), and environment (groundwater pollution by brine) of salt cavern oil storage are worth examining to improve the efficiency of oil storage. Against this background, this work presented an operating mode of salt cavern oil and gas co-storage and using natural gas displacement for petroleum recovery. A gas-oil two-phase flow model with gas dissolution and exsolution was proposed to evaluate the application prospects of the new method precisely. Numerical studies indicated that the gas void fraction at the wellhead under quasi-steady state conditions is approximately 0.153, which belongs to bubbly flow, and the pressure at the wellhead of the central tube increased from 5.54 to 6.12 MPa during the entire transient flow stage, with an increase of 10.47%. Compared to the traditional method of using brine as the working fluid, the pump pressure rises from 2.92 to 14.01 MPa. However, if the new mode can be linked with the salt cavern gas storage and when the initial wellhead gas pressure exceeds 13 MPa, the energy consumption of the new method will be lower than that of the traditional brine-based operational mode. A new empirical formula is proposed to determine the two-phase flow pattern under different operating parameters. A special focus was given to energy consumption for oil recovery, which grows roughly in accordance with the operating pressure and oil recovery rate. However, the energy cost per volume of crude oil remains almost unchanged. This work provided a new solution for the serious brine problem and is expected to achieve petroleum recovery through natural gas displacement.

© 2025 The Authors. Publishing services by Elsevier B.V. on behalf of KeAi Communications Co. Ltd. This is an open access article under the CC BY license (http://creativecommons.org/licenses/by/4.0/).

1. Introduction

Petroleum is an essential resource for the long-term, steady growth of the national economy. It is also very important for maintaining national crude oil security and keeping crude oil prices steady (Xi et al., 2019). Petroleum accounts for ~30% of global primary energy consumption, remaining the largest single energy source by share (Xu et al., 2024). As a critical component in the energy reserves, it will continue to play a pivotal role in global energy strategies. The replacement with brine for oil storage and recovery is applied for the operation of the salt cavern oil storage.

* Corresponding author.

E-mail address: ttwang@whrsm.ac.cn (T.-T. Wang).

Specifically, storing crude oil in the cavity to replace brine or injecting brine to replace crude oil realizes the recovery and storage of petroleum (Zhang et al., 2017). However, due to strict control of groundwater and geographical limitations that salt caverns are far from the coast in countries such as China (Liao et al., 2024), it is much more difficult to obtain sufficient and saturated brine, which also limits the rapid development of underground salt cavern oil storage. Moreover, in U.S., the use of aquifers for brine extraction and injection also brings environmental risks, and these accompanying groundwater monitoring measures will significantly increase oil storage costs (Hinkebein, 2003). Against this background, this work proposed an operating mode of petroleum and gas co-storage and using natural gas displacement for petroleum recovery (PGCS) (as shown in Fig. 1).

Compared to traditional methods, this method offers the following advantages.

- (1) Feasible technology: This new operating mode is similar to the gas injection for debrining in the development of salt cavern gas storage (SCGS) (Xie et al., 2023), with mature ground technology and accumulated experience.
- (2) Wide sources of working fluid: Compared to using brine as the working fluid, natural gas has a wide range of sources and lower costs. For instance, Jintan, China's Salt Cavern Gas Storage, has injected and produced more than 13 billion cubic meters of natural gas, and it may be the site of future oil storage projects (Yang et al., 2015). From a geological aspect, the lack of aquifers near oil storage has been a severe problem for many years (Williams et al., 2022). In terms of policy, strict control of groundwater in regions such as China remains a significant challenge for flexible sources of brine (Liao et al., 2024; Wei et al., 2024).
- (3) Operational safety: Using brine displacement for petroleum recovery, unsaturated brine (derived from seawater or aquifer) will cause resolution of the surrounding rock salt, changing the original shape of the cavity and increasing the risk of mechanical instability (Tackie-Otoo and Haq, 2024). Using natural gas as the working gas can avoid such problems altogether and has more significant advantages for the sustained secure functioning of salt cavern oil storage.
- (4) Environmental benefits: The new mode can achieve complete recovery or recycling of natural gas. The traditional method requires a significant annual investment for monitoring and protecting groundwater (Wang et al., 2023). Additionally, the co-storage of crude oil and natural gas can achieve nearly 100% utilization of the underground space (Li et al., 2022). The storage ratio between natural gas and crude oil can be more freely adjusted according to market and peak demand.

Compared to using brine as a working fluid, the mechanism of using natural gas is more complex. Due to the high solubility of natural gas, a significant quantity of natural gas dissolves in crude oil during the storage period. However, as the oil is extracted, the pressure decreases significantly, causing a large amount of gas to separate from the crude oil and form a gas–liquid two-phase flow in the central tube (Sun et al., 2019). Compared to brine, the density of natural gas is mainly influenced by temperature and pressure, and its compressibility is much higher. Therefore, it is urgent to establish a flow and thermal model to precisely characterize this complex process and quantitatively evaluate the feasibility and application prospects of this new method.

The core of such a comprehensive model mainly includes two aspects: multiphase flow and heat transfer within the wellbore. The existing studies of multiphase flow in wellbore appeared in the petroleum industry, such as multiphase flow after accidental gas influx during drilling (Sun et al., 2017), multiphase flow in oil and gas production (Lou et al., 2023), etc. Examining the slip velocity among various phases and the frictional pressure loss in multiphase flow, Nickens (1987), Meng et al. (2015), and Chaves et al. (2022) numerically solved the governing equations of gas and liquid phases, achieving a complete multiphase flow simulation in the wellbore. Ekrann and Rommetveit (1985) and Sun et al. (2019) further considered the mechanism of gas dissolution and exsolution, treating the dissolved gas phase as an additional component, and proposed a two-phase flow model for oil and gas to examine the effects of gas dissolution and exsolution on multiphase flow characteristics within the wellbore. Most studies addressing the heat transfer in cavity have only focused on SCGS and CAES (Perera, 2023). Although there are mature models for flow and heat transfer in pipelines as references, these models are relatively independent and cannot be fully applicable to the engineering scenarios of petroleum recovery from salt caverns through natural gas displacement. Meanwhile, very little is currently known about the interrelationship among heat transfer, multiphase flow, and gas

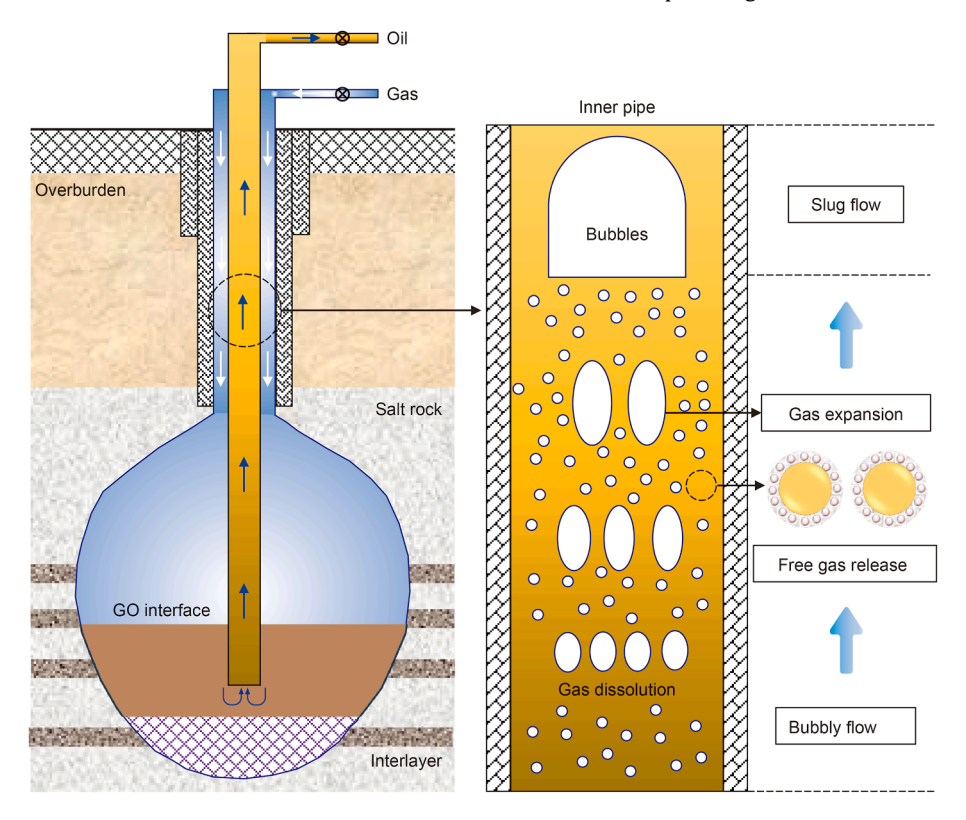


Fig. 1. Schematic of petroleum recovery through natural gas displacement, and formation mechanism of gas-oil two-phase flow during gas injection for oil recovery.

dissolution and exsolution, which may pose significant challenges to the prediction of wellbore flow parameters.

To address the issues of brine source, energy consumption, redissolution of surrounding rock, and environmental impact during the functioning of salt cavern oil storage, this work presented an operating mode of petroleum recovery from salt cavern through natural gas displacement. A systematic mathematical model is constructed to quantitatively and accurately evaluate the application prospects of the new method. Subsequently, numerical simulations were performed to elucidate the intricate link among multiphase flow in the central tube, heat transfer, and gas dissolution/exsolution. Furthermore, a detailed comparison was conducted between using natural gas and brine as working fluids, and the engineering feasibility of the new method was demonstrated. Finally, a special focus was given to the impact of operating pressure and crude oil recovery rate on oil recovery energy consumption. This work provides new solutions for the serious brine problem and is expected to achieve the commercialization of petroleum recovery through natural gas displacement.

2. Model development

This section presents a gas—oil two-phase flow model with gas dissolution and exsolution. Modeling the complex process requires a series of simplified assumptions, as follows: (1) The fluid flow is considered one-dimensional along the wellbore direction. Fluid-related variables are continuous and differentiable functions of space and time. (2) The stored natural gas only considers methane as a single component, neglecting the influence of trace gas components on thermophysical properties such as gas density, viscosity, and specific heat. (3) It is assumed that interphase heat transfer is sufficiently rapid to achieve instantaneous local thermal equilibrium, ensuring that free gas, dissolved gas, and oil at the same depth share identical temperatures. (4) Gas exsolution is assumed to be an instantaneous process.

2.1. Fluid flow

The system's flow can be categorized into a single-phase flow of natural gas in the annulus, natural gas displacing brine in the salt cavern, and a two-phase flow within the central tube.

2.1.1. Gas flow in the annulus

Taking into account the fluctuation of gas density in relation to temperature and pressure, the gas flow can be simplified as onedimensional transient flow, and the governing equations can be articulated as follows:

$$\frac{\partial}{\partial t}(A_{a}\rho_{a}) + \frac{\partial}{\partial z}(A_{a}\rho_{a}\nu_{a}) = 0 \tag{1}$$

$$\frac{\partial}{\partial t}(A_{a}\rho_{a}v_{a}) + \frac{\partial}{\partial z}\left(A_{a}\rho_{a}v_{a}^{2}\right) + \frac{\partial}{\partial z}(A_{a}p_{a}) = -f\frac{A_{a}\rho_{a}v_{a}^{2}}{2\left(d_{ci} - d_{po}\right)} + A_{a}\rho_{a}g \tag{2}$$

where A_a is the cross-sectional area of the annulus, m^2 ; ρ_a is the density of the fluid in the annulus; v_a is the flow velocity of liquids in the annulus; t is the time, s; t is the depth, t is the fluid pressure in the annulus, t is the flow friction coefficient, that can be calculated by the model presented by Wang et al. (2014); t is the inner diameter of the casing, t is the outer diameter of the central tube, t is the gravitational acceleration, t is

2.1.2. Natural gas displacement of brine in salt cavern

Given that the diameter of the salt cavern cavity much exceeds that of the wellbore, it may be inferred that the flow velocity of natural gas within the cavity is zero. Therefore, the pressure distribution inside the cavity can be expressed as follows:

$$\frac{\partial p_{a}}{\partial z} = \begin{cases} \rho_{g}g & (H \le H_{go}) \\ \rho_{o}g & (H > H_{go}) \end{cases}$$
(3)

where $\rho_{\rm g}$ and $\rho_{\rm o}$ are the densities of free gas and crude oil, respectively, kg/m³, $\rho_{\rm g}$ can be calculated by PR equation; $H_{\rm go}$ is the depth of gas–oil interface, m.

2.1.3. Gas-oil two-phase flow in the central tube

In the new mode, the mass exchange between the dissolved gas and free gas in the central tube is highly related to changes in temperature and pressure. Upon the extraction of crude oil, the gas solubility in the crude oil will decrease with the reduce in pressure, causing the dissolved gas to separate from the oil phase (Sun et al., 2019). The continuity equations for free gas and dissolved gas can be derived in accordance with the concept of mass conservation as follows.

Free gas:

$$\frac{\partial}{\partial t} (A_{p} E_{g} \rho_{g}) = \frac{\partial}{\partial z} (A_{p} E_{g} \rho_{g} \nu_{g}) + m_{g}$$
(4)

Dissolved gas:

$$\frac{\partial}{\partial t} \left(A_{\rm p} E_{\rm o} \rho_{\rm o} c_{\rm g} \right) = \frac{\partial}{\partial z} \left(A_{\rm p} E_{\rm o} \rho_{\rm o} c_{\rm g} \nu_{\rm o} \right) - m_{\rm g} \tag{5}$$

where A_p is the cross-sectional area of the central tube, m^2 ; E_g and E_{o} are the gas void fraction and liquid holdup, respectively; ν_{g} and v_0 are the flow velocities of free gas and crude oil in the central tube, respectively, m/s; c_g is the mass fraction of dissolved gas; m_g is the rate at which dissolved gas is converted into free gas per unit length, kg/(m·s). Rommetveit et al. (1989) concluded that the source term $m_{\rm g}$ is a function of temperature, pressure, gas velocity, and bubble size and presented a calculated method of $m_{\rm g}$ based on the convective diffusion analytical solution proposed by Ruckenstein and Davis (1970). Although this method can make the results more accurate, there may be inevitable numerical dissipation, significantly increasing computational costs. This work uses the source term expression proposed by Sun et al. (2019), which assumes that the separation of dissolved gas attributed to the changes in pressure and temperature is instantaneous. Consequently, the source term can be articulated as follows:

$$m_{\rm g} = \frac{\partial}{\partial t} \left(A_{\rm p} E_{\rm o} \rho_{\rm o} c_{\rm g} \right) + \frac{\partial}{\partial z} \left(A_{\rm p} E_{\rm o} \rho_{\rm o} c_{\rm g} \nu_{\rm o} \right) \tag{6}$$

The liquid phase in the central tube is composed of crude oil and dissolved gas, and the transition from dissolved gas to free gas can also cause changes in the flow parameters of crude oil. The mass conservation equation of crude oil can be articulated as follows:

$$\frac{\partial}{\partial t} \left(A_{\mathbf{p}} E_{\mathbf{o}} \rho_{\mathbf{o}} - A_{\mathbf{p}} E_{\mathbf{o}} \rho_{\mathbf{o}} c_{\mathbf{g}} \right) = \frac{\partial}{\partial z} \left(A_{\mathbf{p}} E_{\mathbf{o}} \rho_{\mathbf{o}} \nu_{\mathbf{o}} - A_{\mathbf{p}} E_{\mathbf{o}} \rho_{\mathbf{o}} c_{\mathbf{g}} \nu_{\mathbf{o}} \right) \tag{7}$$

The dynamic distribution and transit of free gas and crude oil affect both the frictional pressure drop and the static liquid column pressure, due to fluctuations in the average density of the mixture. The momentum conservation equation for fluids in the central tube considering slip velocity between different phases can be expressed as follows:

$$\sum_{i=g,o} \frac{\partial}{\partial t} (A_{p} E_{i} \rho_{i} v_{i}) + \sum_{i=g,o} \frac{\partial}{\partial z} (A_{p} E_{i} \rho_{i} v_{i}^{2}) + \frac{\partial}{\partial z} (A_{p} p_{p}) = -f \frac{A_{p} \rho_{m} v_{m}^{2}}{2d_{pi}} + A_{p} \rho_{m} g$$
(8)

where p_p is the fluid pressure in the central tube, Pa; d_{pi} is the inner diameter of the central tube, m; ρ_m is the average density of multiphase mixtures, kg/m³; ν_m is the average velocity of multiphase mixtures, m/s.

2.2. Heat transfer

2.2.1. Heat transfer in the annulus

The transient gas flow in the annulus significantly affects heat transfer. The gas flow process entails the transformation of internal energy, kinetic energy, and potential energy. Simultaneously, it engages in intricate heat exchange with the ambient environment. The energy conservation equation can be articulated with the specific enthalpy of the fluid as the focal point of the study.

$$\frac{\partial}{\partial t} \left[A_{a} \rho_{g} \left(U + \frac{1}{2} v_{a}^{2} \right) \right] + \frac{\partial}{\partial z} \left[A_{a} \rho_{g} v_{a} \left(H + \frac{1}{2} v_{a}^{2} \right) \right] = - A_{a} \rho_{g} v_{a} g + Q_{e}$$
(9)

where U is the specific internal energy, J/kg; H is the specific enthalpy, J/kg; Q_e is the heat flow rate from the surrounding environment to the wellbore, W/m.

According to the gas thermodynamic theory, Eq. (8) can be further simplified as follows. The specific steps can be found in the work we have published previously (Liao et al., 2022, 2023).

$$\begin{split} A_{a}\rho_{g}C_{V,g}\frac{\partial T_{a}}{\partial t} - A_{a}\left(\rho_{g}\mu_{JT}C_{V,g} + 1\right)\frac{\partial p_{a}}{\partial t} + A_{a}\rho_{g}\nu_{a}\left(\frac{\partial\nu_{a}}{\partial t} + C_{V,g}\frac{\partial T_{a}}{\partial z}\right) \\ - \mu_{JT}C_{V,g}\frac{\partial p_{a}}{\partial z} + \nu_{a}\frac{\partial\nu_{a}}{\partial z}\right) \\ = -A_{a}\rho_{g}\nu_{a}g - \pi d_{pi}U_{p}\left(T_{a} - T_{p}\right) + \pi d_{ci}U_{a}\left(T_{e,0} - T_{a}\right) \end{split} \tag{10}$$

where $C_{V,g}$ is the specific heat capacity of gas, $J/(kg \cdot {}^{\circ}C)$; T_a , T_p , and T_e are the temperature of the annulus, central tube, and formation, respectively, ${}^{\circ}C$; μ_{JT} is the Joule–Thomson coefficient, K/Pa; U_p is the comprehensive heat transfer coefficient between the central tube and annulus, $W/(m^2 \cdot {}^{\circ}C)$; U_a is the total heat transfer coefficient between the annulus and surrounding environment, $W/(m^2 \cdot {}^{\circ}C)$.

2.2.2. Heat transfer in the central tube

Considering the convective heat transfer between the central tube and the annulus, and heat caused by flow friction, the energy conservation equation for the mixed fluids in the central tube can be obtained as follows (Sun et al., 2017):

$$\begin{split} A_{p}(\rho C)_{m} \frac{\partial T_{p}}{\partial t} + \frac{1}{2} \sum_{i=g,o} \frac{\partial}{\partial t} \left(A_{p} E_{i} \rho_{i} v_{i}^{2} \right) - \frac{\partial \left(A_{p} p_{p} \right)}{\partial t} \\ &= -A_{p}(\rho C \nu)_{m} \frac{\partial T_{p}}{\partial z} - \frac{1}{2} \sum_{i=g,o} \frac{\partial}{\partial t} \left(A_{p} E_{i} \rho_{i} v_{i}^{3} \right) - A_{p} \sum_{i=g,o} (\rho_{i} \nu_{i}) g \cos \theta \\ &+ A_{p} f \frac{\rho_{m} \nu_{m}^{2}}{2 d_{pi}} \nu_{m} + \pi d_{pi} U_{p} \left(T_{a} - T_{p} \right) \end{split}$$

$$(11)$$

The first three terms of Eq. (10) represent the changes in

internal energy, kinetic energy, and pressure energy of the fluid in the central tube, respectively. The three items in the second row represent the changes in internal energy, kinetic energy, and potential energy caused by fluid flow, respectively. The two items in the third row represent the heat generated by flow friction and heat exchange with the annulus, respectively.

2.3. Auxiliary equations

To make the governing equations of fluid flow and heat transfer closed and solvable, it is necessary to establish corresponding auxiliary equations. The auxiliary equations primarily encompass the density and viscosity models of crude oil and the natural gas solubility model, which can be found in the literature (Wang et al., 2025).

3. Numerical solution and verification

3.1. Numerical solution

The classic pressure assumption-correction method is commonly used to solve the multiphase flow and heat transfer equations (Wang et al., 2016). Based on this method, this work embedded the state equation and gas solubility equation of crude oil. The particular discrete format and derivation method are given in Appendix A and Appendix B.

In the solution of multiphase fluid flow and heat transfer within the wellbore, the continuity of the temperature field is smoother compared to other flow parameters; thus, the convergence speed is faster. The calculation of the pressure field is the core of this work. This work used the classic pressure assumption-correction method to solve the model, and the flow chart is illustrated in Fig. 2. Three iterations make up the complete calculation process: the iterative solution of the temperature field, the iterative solution of the pressure field, and the iterative solution of the multiphase flow parameters. The following are the precise steps.

- (1) Assuming the distribution of temperature and pressure fields in the wellbore at time k, the values at time k-1 are typically utilized for the initial iteration, while the results from the preceding iteration are employed for subsequent iterations.
- (2) Based on the assumed temperature field distribution, solving the natural gas solubility equation to obtain the conversion rate of dissolved gas to free gas per unit length (m_g) .
- (3) Solving the drift model to obtain the gas slip velocity (v_{gr}).
- (4) Solving the continuity equations for free gas, dissolved gas, and crude oil and obtaining the gas void fraction and flow velocity of free gas and crude oil, as well as the mass fraction of dissolved gas (Appendix A).
- (5) Using the momentum conservation equation to obtain the pressure field distribution in the wellbore and iteratively updating the flow parameters of oil and gas phases.
- (6) Assessing whether the pressure distribution satisfies the convergence criteria. If it does not, return to Step (1).
- (7) Solve the thermal model in the annulus and central tube (Appendix B). Ascertain if the temperature distribution satisfies the convergence criteria. If it fails to do so, revert to Step (1).
- (8) Solving for the next step.
- (9) Repeating the above steps until all time steps are solved.

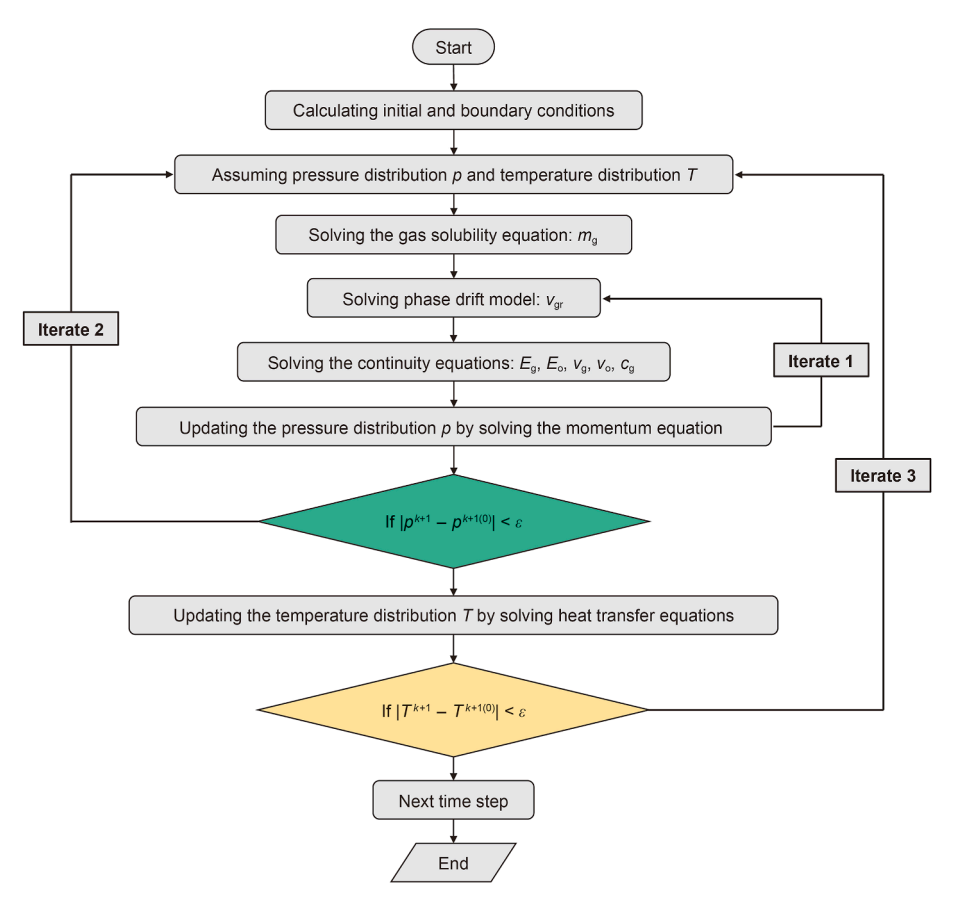


Fig. 2. Flow chart of the calculation process.

3.2. Model verification

This work first proposed a new operating mode of PGCS. As there are currently no engineering cases worldwide, it is different to thoroughly verify the new model presented in this work through field monitoring data. For the study of the wellbore temperature field, we have demonstrated the accuracy of the model in previous studies (Liao et al., 2023), and the gas—oil two-phase flow under gas dissolution and exsolution conditions requires further verification.

Once gas influxes into the wellbore, a gas–liquid two-phase flow will be formed if the oil-based drilling fluid is used for drilling, in which gas dissolution and exsolution in the oil phase are involved. This situation has the same characteristics as the new method of oil recovery mode proposed in this work. Therefore, a case of deep-water drilling in South China Sea collected from literature is obtained to validate the new model. The water depth is 1455 m and the well structure is $D=914.4 \, \mathrm{mm} \times 1554 \, \mathrm{m} + 660.4 \, \mathrm{mm} \times 2180 \, \mathrm{m} + 476 \, \mathrm{mm} \times 2730 \, \mathrm{m} + 444.5 \, \mathrm{mm} \times 3260 \, \mathrm{m$

311 mm \times 3561 m. The drilling mud density is 1.35 g/cm³ and the flow rate is 63 L/s. The basic parameters used for model verification are shown in Table 1. Detailed information can be found in the literature (Sun et al., 2019).

Based on the primary data in Table 1, the gas-oil two-phase flow model proposed in this work was used to calculate the multiphase flow behavior in the wellbore. As shown in Fig. 3, the solid and dashed blue lines represent the dissolved gas mass fraction at 1000 and 3000 s, respectively. Once gas influx occurs, free gas enters the wellbore from the formation and is completely dissolved in an oil-based drilling fluid. As the drilling fluid gradually returns upwards and the pressure decreases, the gas solubility in the drilling fluid tends to saturate. Then, the dissolved gas begins to separate out, forming a gas-liquid two-phase flow in the upper part of the wellbore.

Due to the lack of reliable downhole real-time measurement devices, it is difficult to directly verify the model presented in this work through the complex multiphase flow parameters in the wellbore. However, the pit gain on the ground can indirectly reflect

Table 1Basic parameters in the model verification.

Parameter	Value	Parameter	Value
Well depth	3510 m	Geothermal gradient	3.79 °C/100 m
Outer diameter of the casing	444.5 mm	Inner diameter of the casing	420.5 mm
Depth of casing	3260 m	Diameter of the borehole	311 mm
Outer diameter of the string	149.2 mm	Inner diameter of the string	128.1 mm
Kick intensity	60 kg/m ³	Density of the drilling fluid	1.35 g/cm ³

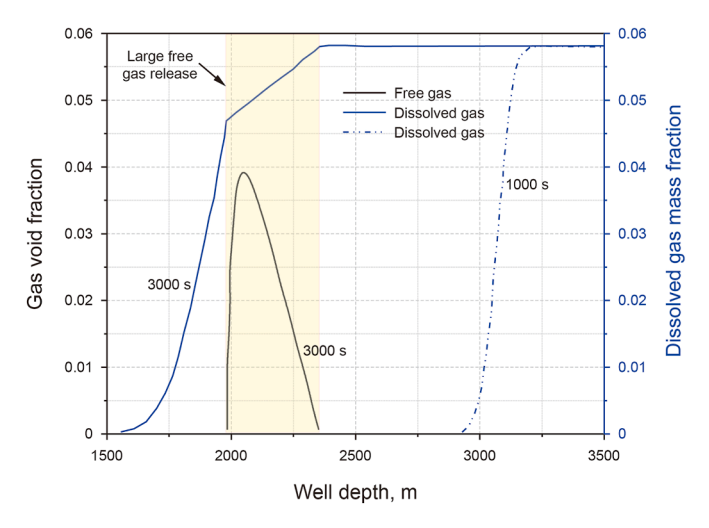


Fig. 3. Distributions of free gas and dissolved gas in the central tube.

the multiphase flow downhole. Fig. 4 shows the comparison of pit gain between the model prediction and field data. The new model can effectively predict the multiphase flow behavior in the wellbore, with a prediction error of only 5.92% for the pit gain. The multiphase flow model presented in this work was validated based on limited data. If the new mode can be applied in the field in the future, field monitoring data, such as downhole pressure and fluid volume fraction at the wellhead, can better validate this model.

4. Feasibility analysis of the new mode

To quantitatively evaluate the feasibility of oil recovery through natural gas displacement in salt cavern, and demonstrate the technical advantages and potential shortcomings of the new method, this study examines a salt cavern gas storage facility situated in China as the engineering application. The shape of the cavern, as determined by Sonar measurement, is illustrated in Fig. 5. Compared to the operation of salt cavern gas storage or oil storage, the most prominent feature of this new operation mode is the multiphase flow and pressure control in the central tube during gas injection for oil recovery. Its static storage stage is

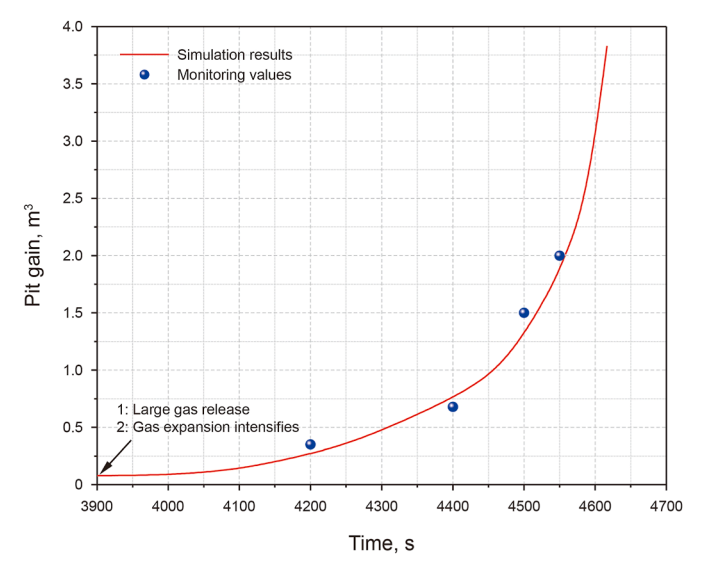


Fig. 4. Comparison of pit gain between the model prediction and field data.

almost the same as that of oil/gas storage. Therefore, numerical simulations were performed to gain a comprehensive understanding of the multiphase flow characteristics during gas injection for oil recovery, along with the variations in wellbore temperature and pressure profiles. The wellbore structure of salt cavern gas storage and oil storage is slightly different due to the significant difference in viscosity between gas and crude oil. This work used the pipe structure and size from a salt cavern oil storage in the U. S., and the main simulation data is shown in Table 2.

4.1. Results

4.1.1. Transient temperature profile

Real-time prediction and monitoring of the temperature profile in the wellbore can provide necessary data support for the design of ground crude oil treatment. Based on the initial conditions, the fluids in the central tube and annulus have undergone sufficient heat exchange with the surrounding rock. Its temperature is essentially aligned with the formation temperature. As the beginning of gas injection for oil recovery, the thermal equilibrium is disrupted, and the temperature field in the wellbore changes.

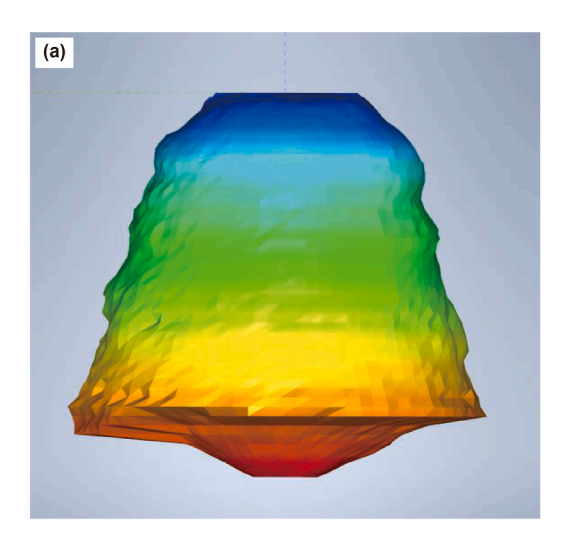
Fig. 6 shows the temperature profiles of the fluids in the central tube (solid line) and annulus (dashed line) at 100, 200, 400, and 800 s. It can be clearly observed that the gas in the wellbore gradually flows downwards the salt cavern (the depth corresponding to the temperature valley gradually decreases). On the one hand, injecting gas continuously absorbs heat from surrounding formations: meanwhile, rapid gas compression (Joule-Thomson effect) will cause the gas temperature to increase gradually. However, this increasing trend will gradually slow down and eventually reach a quasi-equilibrium state. The increase in temperature of the gas in the annulus will also reduce the thermal energy dissipated from the crude oil in the central tube to the ambient environment. The fluid temperature in the central tube gradually increases, and the outlet temperature of the crude oil gradually increases from 23.40 to 40.36 °C, with an increase of 72.48%. For the entire gas injection for the oil recovery process, the duration of this transient process is relatively short and can be ignored in engineering.

4.1.2. Transient pressure profile

The pressure variation during the injection-production operation process has vital significance for the optimization of surface compressors. Fig. 7 illustrates the pressure profiles of the fluids in the central tube (solid line) and annulus (dashed line) at 100, 200, 400, and 800 s. The attached figure illustrates the temporal change of wellhead pressure. The fluid pressure in the central tube progressively escalates with time. The fundamental reason is the decrease in the static liquid column pressure of the mixed fluid. primarily due to both the continuous increase in crude oil temperature, which reduces its density, and the evolving multiphase flow within the wellbore, where the void fraction of free gas is progressively rising. As shown in the attached figure, the pressure distribution also tends to stabilize with the temperature and multiphase flow characteristics. The pressure at the wellhead of the central tube increased from 5.54 to 6.12 MPa during the entire transient flow stage, with an increase of 10.47%. Compared with the significant changes in pressure of the central tube, the annular pressure hardly changes over time, mainly due to the small gas density; temperature changes thus have little impact on the overall pressure profile.

4.1.3. Gas-oil two-phase flow behavior

Compared to the traditional method of using brine as the working fluid, natural gas with a broader range of sources will



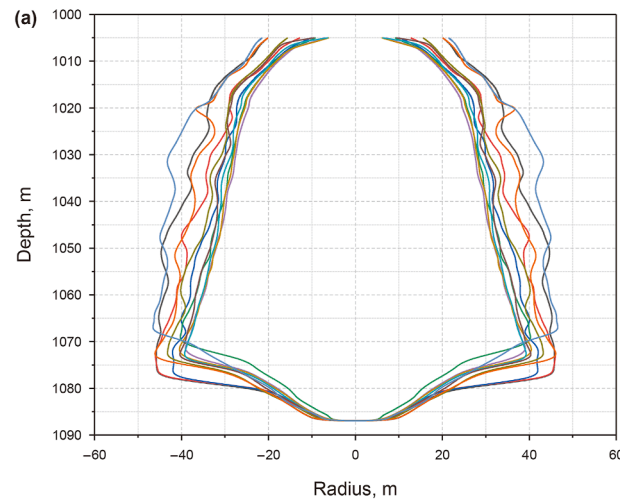


Fig. 5. The shape and plan of the salt cavern obtained by Sonar measurement.

Table 2Basic parameters in the model performance.

Parameter	Value	Parameter	Value
Outer diameter of the inner tube	237.05 mm	Inner diameter of the inner tube	250.54 mm
Outer diameter of the casing	339.72 mm	Inner diameter of the casing	317.08 mm
Depth of the inner tube	1070 m	Depth of the casing	1000 m
Surface temperature	20 °C	Geothermal gradient	3.0 °C/100 m
Injection temperature of gas	30 °C	Operating pressure	15.5 MPa
Gas-oil interface	1030 m	Standard density of crude oil	950 kg/m ³

form a gas-liquid two-phase flow in the central tube during the oil recovery process. Fig. 8 shows the free gas void fraction in the central tube at 100, 200, 400, 800, and 1200 s. It can be observed that the free gas void fraction in the central tube gradually increases over time and eventually tends towards a steady state. This is mainly because as the crude oil returns upwards, the decrease in fluid pressure causes a large amount of dissolved gas to separate out; besides, the free gas expands continuously. The gas void fraction at the wellhead under quasi-steady state conditions is

~0.153, which belongs to bubbly flow (Liao et al., 2019). Bubbly flow is relatively easy to handle, and conventional gravity separation towers can achieve rapid separation of free gas and oil. This also indirectly demonstrates the engineering feasibility of the oil recovery mode and will not bring additional costs to the ground gas—liquid separation.

The separation of dissolved gas from crude oil is the direct cause of the formation of gas-liquid two-phase flow in the central

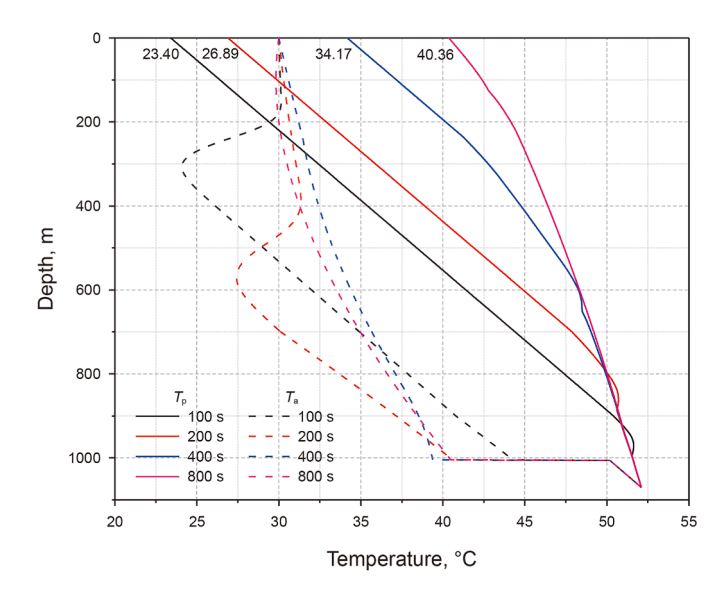


Fig. 6. Temperature profiles of the fluids in the central tube (solid line) and annulus (dashed line) at 100, 200, 400, and 800 s.

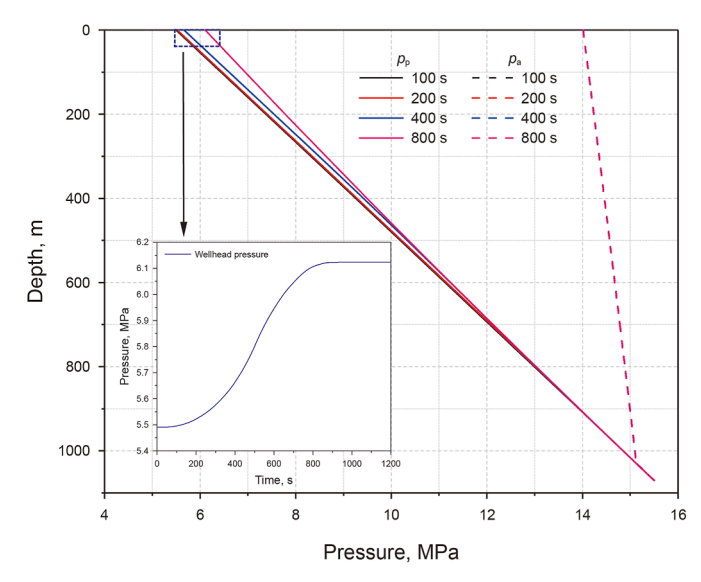


Fig. 7. Pressure profiles of the fluids in the central tube (solid line) and annulus (dashed line) at 100, 200, 400, and 800 s. The attached figure shows the variation of wellhead pressure over time.

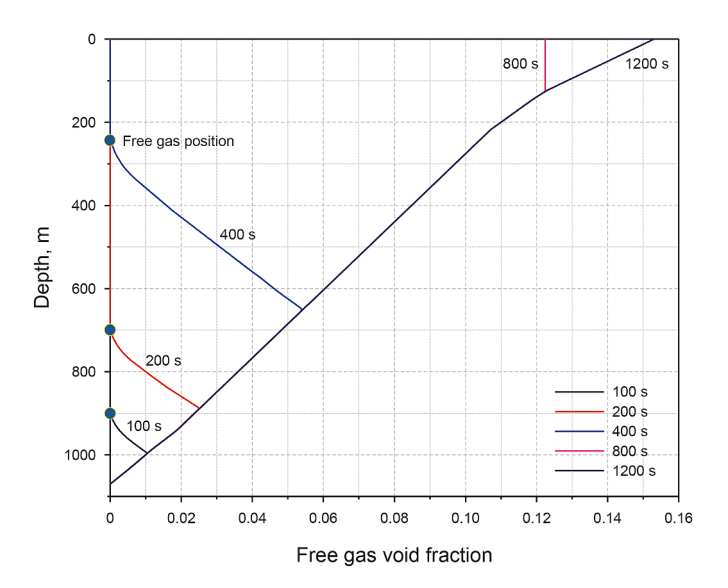


Fig. 8. Free gas void fraction in the central tube at 100, 200, 400, 800, and 1200 s.

tube. Fig. 9 further presents the mass fraction profiles of dissolved gas in the crude oil at 100, 200, 400, 800, and 1200 s. It can be found that free gas continuously separates out from the crude oil that saturated dissolved gas during the upward flow process. After reaching a steady state, the crude oil at the wellhead still remains saturated with dissolved gas under in-situ temperature and pressure conditions. Once the pressure decreases in the ground pipeline, dissolved gas will be further separated out, degassed, and gas-liquid separated on the ground; thus, it is essential.

4.2. Comparison with conventional mode

4.2.1. Pump pressure

Compared to using brine as the working fluid, natural gas requires higher energy consumption during oil recovery due to its low density and strong compressibility. Fig. 10 shows the comparison of brine and natural gas as the working fluid. It can be found that at the same oil recovery rate, using gas as the working

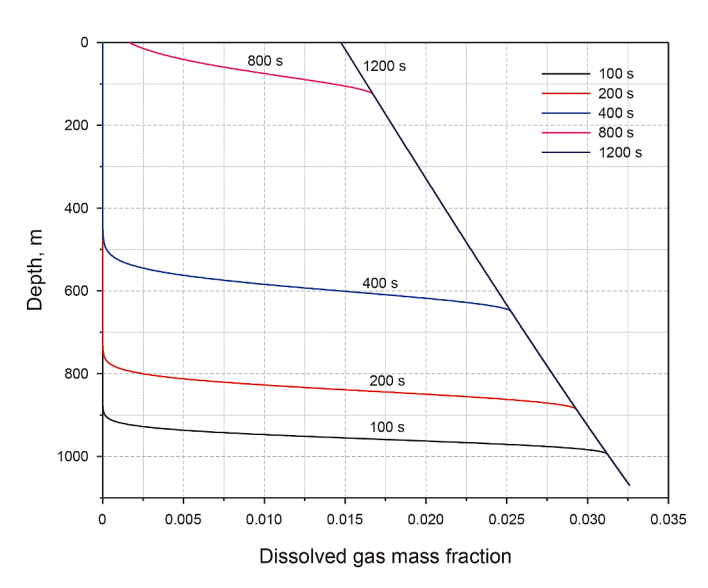


Fig. 9. Mass fraction profiles of dissolved gas in the crude oil at 100, 200, 400, 800, and 1200 s.

fluid results in higher pressure in the central tube and annulus. It is mainly because the gas—liquid two-phase flow formed in the central tube will reduce the static liquid column pressure, resulting in a higher pressure in the central tube. The annulus, while is a pure gas column with a smaller pressure gradient. Compared to traditional methods, the pump pressure increased from 2.92 to 14.01 MPa.

4.2.2. Energy consumption

For the operation mode of oil recovery through natural gas displacement, the operating pressure and the recovery rate of crude oil are significant concerns in engineering, especially the operating energy consumption under different operating conditions. The energy loss during operation mainly comes from the ground compressor. Currently, a simple prediction method is generally used as follows, which is directly related to gas mass flow rate, compressor inlet and outlet pressure, etc.

$$\begin{cases}
P_{W} = \frac{q_{g}}{\eta} \frac{u}{u - 1} Z_{1} \frac{R}{M} T_{1} \left[\left(\frac{p_{2}}{p_{1}} \right)^{\frac{u - 1}{u}} - 1 \right] \\
u = \frac{1}{1 - \frac{k - 1}{\eta k}}
\end{cases} (12)$$

where $P_{\rm w}$ is the power of gas injection compressor, MW; $q_{\rm g}$ is the mass flow rate of natural gas, kg/s; η is the efficiency of the compressor; u is the polytropic index; k is the isentropic index which is generally between 1.2 and 1.4 for natural gas, in this work k=1.3; Z_1 is the compression factor of natural gas at the inlet of the compressor; R is the gas constant, 8.314 J/(mol·K); M is the molar mass of natural gas, kg/mol; T_1 is the temperature of natural gas at the inlet of the compressor, K; p_1 and p_2 are the pressures at the inlet and outlet of the compressor, respectively, MPa.

The energy consumption required per unit volume of crude oil can be calculated using the following formula:

$$E_{\rm W} = \frac{P_{\rm W}}{O_{\rm O}} \tag{13}$$

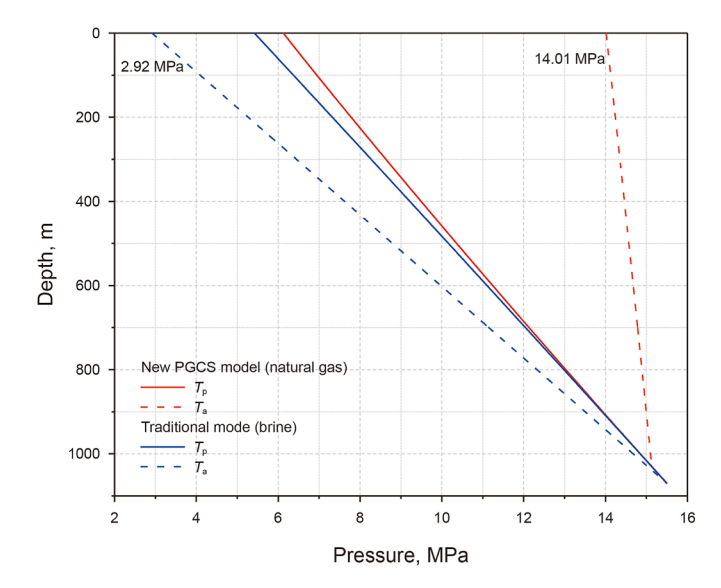


Fig. 10. Comparison of brine and natural gas as the working fluid. The red line represents the new PGCS mode, and the blue line represents the traditional brine-based operational mode.

where E_W is the energy consumption for recovery unit volume of crude oil, MJ/m³; Q_0 is the recovery rate of crude oil, m³/s.

In the new operating mode of oil recovery, the high energy consumption for oil recovery is the most significant disadvantage. However, effectively leveraging the natural gas pressures within the salt cavern gas storage can significantly reduce operational energy consumption. Fig. 11 shows the energy consumption of oil recovery under different initial gas pressures and the comparison with the traditional mode. The energy consumption decreases with the increase in initial gas pressure. Taking the Jintan Gas Storage, China, as an example, to ensure the safety of surrounding rock salt, the wellhead gas pressure is generally maintained within a range of 7-17 MPa. Therefore, when the wellhead pressure of the salt cavern gas storage exceeds the pump pressure required for oil recovery (14.01 MPa), the gas can be directly injected into the salt cavern oil storage for oil recovery without requiring additional pressure via compressors. Comparative analysis indicates that when the initial wellhead gas pressure exceeds 13 MPa, the energy consumption of the new method will be lower than that of the traditional brine-based operational mode. Certainly, under low natural gas pressure conditions, advanced compressor technologies and energy recovery schemes can further minimize the energy consumption of the novel method.

4.2.3. Safety and environmental impact

Compared to brine, natural gas is flammable and poses higher leakage risks, leading to greater environmental and safety impacts in the event of an accident. It imposes stricter requirements on the geological conditions of oil storage facilities. Furthermore, under the new mode, the fluid returning from the wellhead changes from single-phase petroleum to a gas-oil two-phase mixture. As shown in Fig. 8, the gas void fraction at the wellhead is ~0.153. Under the condition of low-pressure operations and rapid extraction, slug flow may develop at the wellhead, significantly increasing the complexity and risks of surface processing. Besides, the presence of slugs can also cause periodic vibration of the pipe string (Bamidele et al., 2021), and further study is needed to determine whether it will cause irreparable harm to the integrity of the wellbore. Therefore, it is recommended that leakage monitoring measures for the wellbore and surface pipelines be enhanced to mitigate the operational risks of the new mode.

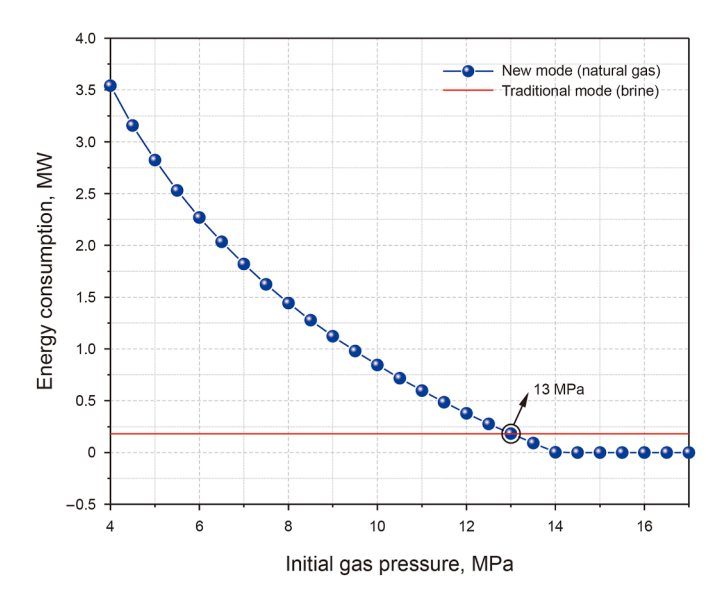


Fig. 11. Energy consumption of petroleum recovery under different initial gas pressures and the comparison with the traditional mode.

Meanwhile, using gas as the working medium may result in the volatilization of light hydrocarbon components from petroleum, this does not compromise the quality of the natural gas, which can still be fully utilized. However, liquid-phase components in petroleum could contaminate the brine, and the extracted brine during petroleum injection may pose environmental risks. For this reason, the United States continues to conduct groundwater hydrocarbon monitoring to prevent contamination of aquifers by reinjected brine (Munson, 2010).

4.3. Sensitivity analysis of the PGCS operation mode

Operating pressure, petroleum recovery rate, and wellhead flow pattern are the key parameters in the novel operational mode, which will influence both the operating conditions and the ground multiphase separation processes for oil, gas, and water. The salt cavern shape might affect the dissolution dynamics of natural gas in petroleum, and this factor exerts a negligible impact on the PGCS mode. Thus, this section will conduct a quantitative analysis of the effects of these three factors on the energy consumption of the new operational mode and the gas content at the wellhead.

4.3.1. Operating pressure

Operating pressure is a critical parameter in the design of PGCS operation mode, and it mainly depends on the depth of the salt cavern, ground stress, and fracturing pressure (Tarkowski, 2019). If the operating pressure is too high, it may lead to the rupture and instability of the cavity (Li et al., 2021). At the same time, if the operating pressure is too low, it may cause uncontrolled rapid contraction of the cavity (Mansouri and Ajalloeian, 2018). Salt cavern gas storage generally needs to set the upper and lower limits of operating pressure. In the new PGCS operation mode, to ensure the long-term stability of the storage, constant pressure operation is generally adopted, that is, keeping the salt cavern pressure basically unchanged during the oil injection, storage, and recovery process.

Fig. 12 shows the gas void fraction in the central pipe at different operating pressures. It can be observed that as the operating pressure decreases, the gas void fraction in the central tube during the oil recovery process increases. This is mainly because the lower the working pressure, the more intense the

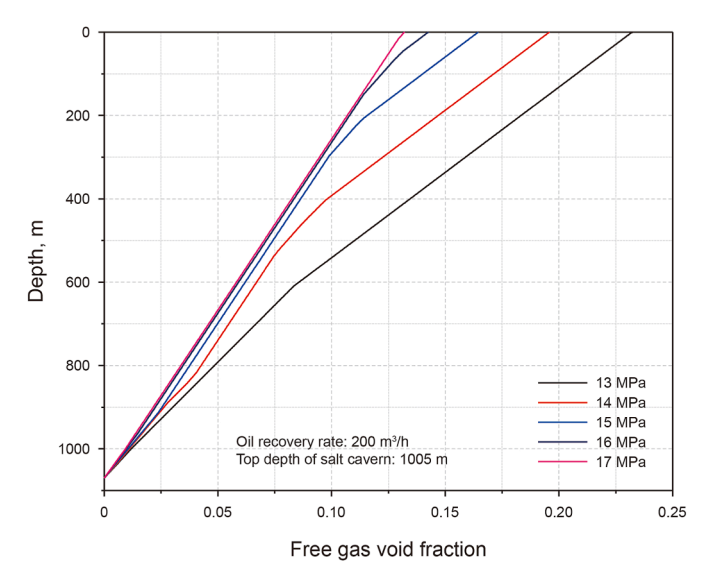


Fig. 12. Gas void fraction profile in the central pipe at the operating pressures of 13, 14, 15, 16, and 17 MPa.

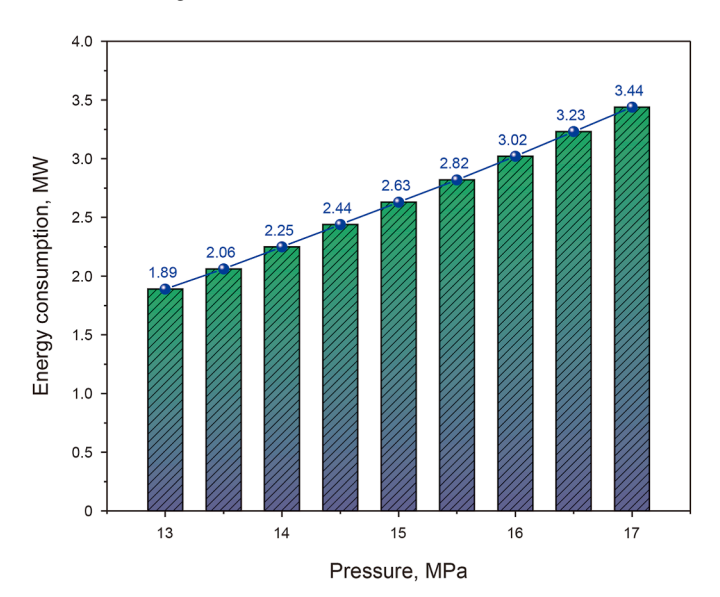


Fig. 13. Energy consumption for oil recovery at different operating pressures. Oil recovery energy consumption increases approximately linearly with the operating pressure.

expansion of free gas, and the higher the gas volume. Therefore, regardless of the stability of the surrounding rock salt and the complexity of multiphase flow in the central tube, a larger operating pressure should be adopted. As shown in Fig. 13, the energy consumption for oil recovery at different operating pressures is further presented. Oil recovery energy consumption increases approximately linearly with the operating pressure. Obviously, the increased operating pressure results in a heightened pressure on the ground compressor. Therefore, in the new PGCS operation mode, it is essential to thoroughly assess many issues, such as economy, safety, and multiphase flow behavior, and then determine a suitable operating pressure for energy storage.

4.3.2. Recovery rate of crude oil

According to the injection-production practice of salt cavern oil storage in the U. S., the oil recovery rate using brine as a working fluid can reach up to 800 m³/h (Munson, 2010). This is due to the fact that the static liquid column pressure of brine can balance most of the crude oil pressure, and only a small pump pressure is required to achieve rapid crude oil extraction. Therefore, whether using gas as the working fluid in the new mode can obtain an acceptable displacement has always been a concern in the engineering community. Fig. 14 shows the gas void fraction in the central pipe at different oil recovery rates. It can be found that as the oil recovery rate increases, the gas void fraction increases. This is mainly due to the fact that the faster the oil recovery rate, the greater the separation rate of dissolved gas from crude oil. Furthermore, the escalation in the oil recovery rate will increase the flow friction, leading to a decrease in the wellbore pressure profile. Therefore, the expansion of free gas is becoming more intense.

Fig. 15 shows the energy consumption and energy consumption per volume for oil recovery at different oil recovery rates. The energy consumption increases with the oil recovery rate; interestingly, the energy consumption per volume of crude oil remains almost unchanged. This also indirectly reflects that the oil recovery rate has a minimal influence on overall energy use. In engineering applications, an appropriate oil recovery rate should be established depending on market demand and the capacity of surface equipment.

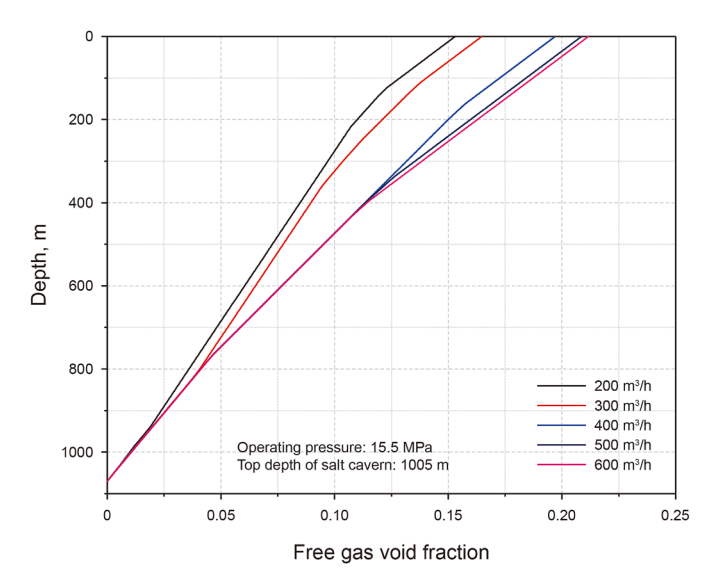


Fig. 14. Gas void fraction in the central pipe at different oil recovery rates.

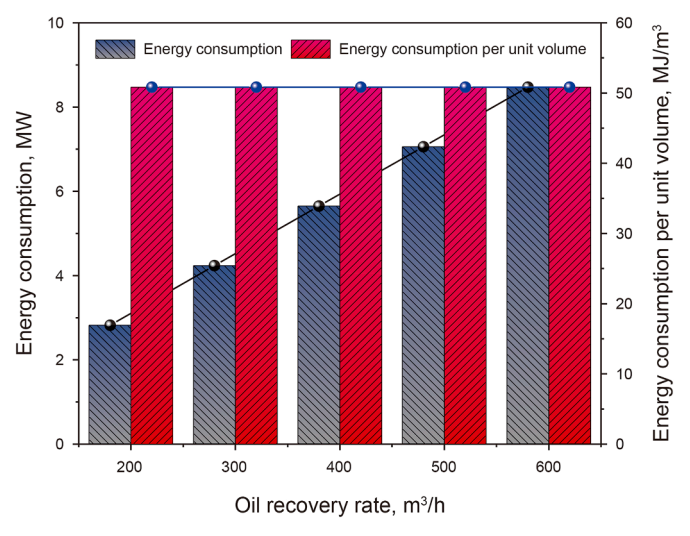


Fig. 15. Energy consumption and energy consumption per volume for oil recovery at different oil recovery rates.

4.3.3. Flow pattern analysis

Fig. 16 illustrates the distribution of gas void fraction at the wellhead under various operating conditions. The gas void fraction at the wellhead diminishes with rising operating pressure and increases with the oil recovery rate. Under conditions of low operating pressure and high oil recovery rate, the gas void fraction in the wellhead produced fluid is higher. Generally, when the gas void fraction is below 0.25, the flow pattern exhibits bubbly flow; that is, the central tube is still filled with crude oil, and the gaseous phase is spread inside the liquid phase as tiny bubbles. When the gas void fraction exceeds 0.25, it exhibits slug flow, where dispersed free bubbles gather to form Taylor bubbles (as shown in Fig. 1). Both the free gas and liquid phases have a significant impact on the pressure gradient.

The separability and operational safety of bubbly flow are far superior to those of slug flow. Therefore, to optimize the operating pressure and oil recovery rate in the novel method for avoiding slug flow at the wellhead, this work proposes an empirical formula to determine the flow pattern boundary between bubbly flow and

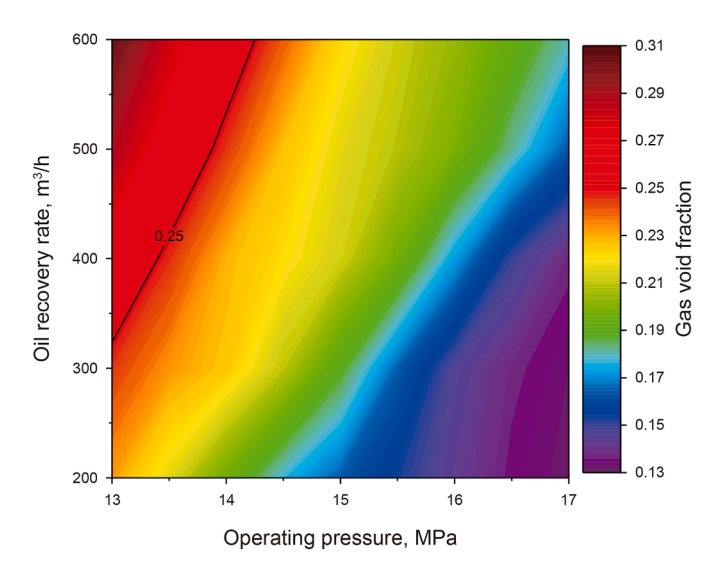


Fig. 16. Wellhead gas void fraction distribution under different operating conditions.

slug flow at the wellhead through data fitting (see in Fig. 17). The coefficient of determination (\mathbb{R}^2) of the formula reaches 0.9986, demonstrating that the model effectively explains the coupling relationship among operating pressure, oil production rate, and flow pattern transitions. Once the commercial operation of the new PGCS operation mode is applied in the future, field engineers can quickly verify the designed operating parameters to prevent the emergence of slug flow in the central tube.

$$Q_0 = 9.6763p^2 - 41.003p - 786.9 \tag{14}$$

where p is pressure. MPa.

Fig. 18 shows the energy consumption for oil recovery under different operating conditions. As we mentioned in Section 4.3.2, the energy usage for oil recovery escalates almost linearly with both the operating pressure and the oil recovery rate. Still, the energy consumption per unit volume of crude oil remains virtually unchanged. When the operating pressure is 13 MPa, the oil recovery rate is $200 \, \mathrm{m}^3/\mathrm{h}$, the energy consumption for oil recovery is

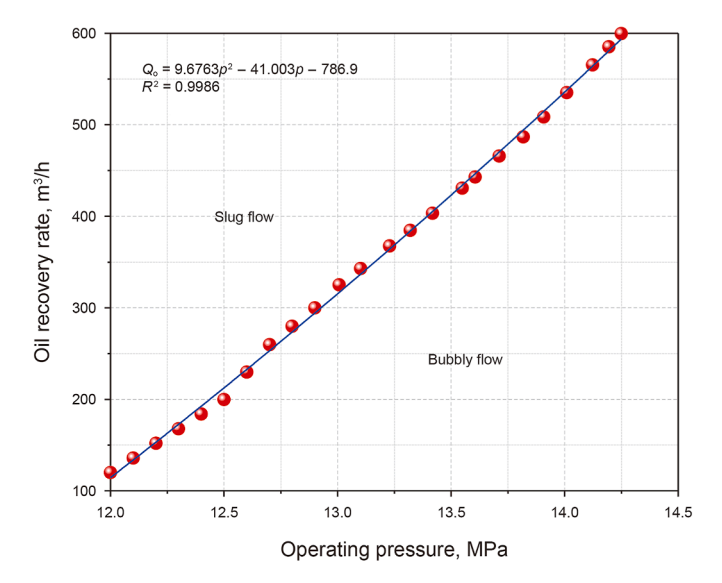


Fig. 17. Flow pattern boundaries of bubbly flow and slug flow under different operating conditions.

1.89 MW. When the operating pressure increases to 17 MPa and the oil recovery rate reaches 600 m³/h, the energy consumption for oil recovery is 10.31 MW, with an increase of 4.45 times. Obviously, energy consumption is only one of the critical factors determining the oil recovery rate. The actual oil recovery rate needs to be determined comprehensively based on factors such as ground equipment processing capacity and market demand.

4.4. Discussion

This work presented a new PGCS operation mode, and a gas-oil two-phase flow model with gas dissolution and exsolution for petroleum recovery from salt cavern through natural gas displacement was proposed. Several empirical relationships, including the gas-oil drift flow relationship, density and viscosity models of crude oil and natural gas solubility model obtained by other researchers, are used in this work. Therefore, the current verification is not fully completed. If real-time monitoring of downhole pressure via pressure while drilling (PWD) technology and measurement of two-phase fluid volume fraction at the wellhead could be achieved in future applications, the model and its empirical parameters can be further optimized. Additionally, this study simplifies the gas dissolution process from upper gas layers into underlying crude oil during gas displacement in salt cavern gas storage, adopting a simplified assumption that the crude oil has reached gas dissolution saturation during prolonged storage. Further research efforts are still required to investigate the dissolution mechanisms under oil-gas co-storage conditions. Future investigations should focus on the long-term stability and gas tightness of the entire system, as well as the impacts of oil-gas coexistence on petroleum quality parameters, particularly including bubble point pressure variations and compositional contamination effects.

The new method solves the challenge of brine source and its additional problems. At the same time, there are still some issues that could be improved. (1) As the pressure of the extracted petroleum decreases, dissolved gas separates out and forms gas—liquid two-phase flow in the wellbore. During low-pressure operations and rapid extraction, slug flow may develop at the wellhead. Consequently, gas—oil separation units are required on the surface to separate the two phases. Excessive gas content further increases separation difficulty and raises separation costs. Therefore, it is recommended to enhance leakage monitoring

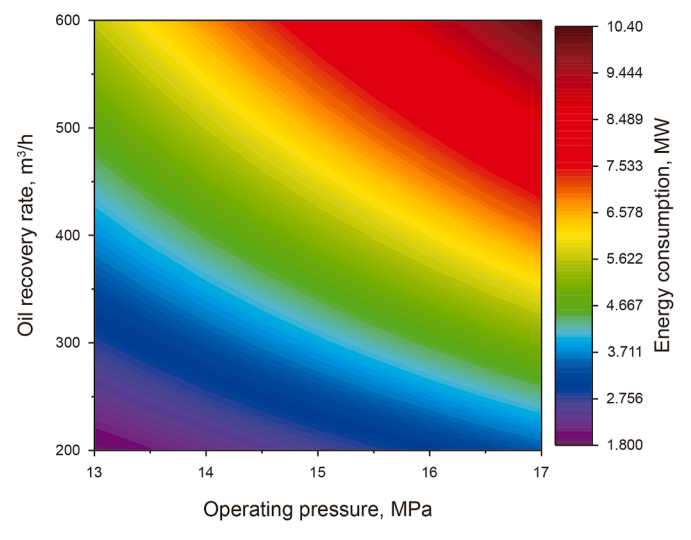


Fig. 18. Energy consumption for oil recovery under different operating conditions.

measures for the wellbore and surface pipelines to mitigate operational risks of the new mode. (2) Using natural gas as the working fluid results in higher energy consumption for oil recovery and hinders achieving a high-displacement effect under equivalent power conditions. Nevertheless, effectively utilizing the natural gas pressure from salt cavern gas storage could substantially reduce operational energy consumption. (3) Due to the much higher viscosity of crude oil than natural gas, scholars have proposed the idea of transforming some poorly sealed salt caverns or brine extraction cavities into salt cavern oil storage (Wei et al., 2023). While in the new PGCS operation mode, it is still necessary to screen and evaluate salt caverns according to the standards of gas storage.

5. Conclusions

This study proposed an operating mode of petroleum recovery from salt cavern through natural gas displacement. Then, a mathematical model is presented considering the gas—oil two-phase flow, transient heat transfer, and gas dissolution/separation to quantitatively and precisely evaluate the application prospects of the new mode.

Feasibility analysis shows that the pump pressure of the compressor is 14.01 MPa in the new mode, while that is 2.92 MPa in the mode of using brine as working fluid. However, if the new mode can be linked with the salt cavern gas storage and when the initial wellhead gas pressure exceeds 13 MPa, the energy consumption of the new method will be lower than that of the traditional brine-based operational mode. From the perspective of security, the gas-liquid two-phase flow formed in the central tube is mainly a bubbly flow. It only develops into slug flow under low operating pressure and fast oil recovery rate, and a new formula has been proposed to calculate this boundary. In the new mode, gas-liquid separation is easy to implement and cost-effective. The energy consumption of oil recovery increases approximately linearly with the operating pressure and oil recovery rate, while the energy consumption per volume remains almost unchanged. Energy consumption is only one of the critical factors determining the oil recovery rate, the actual oil recovery rate needs to be determined comprehensively based on factors such as ground equipment processing capacity and market demand.

CRediT authorship contribution statement

You-Qiang Liao: Writing – original draft, Methodology, Investigation. **Tong-Tao Wang:** Writing – review & editing, Supervision. **Tao He:** Validation, Methodology. **Dong-Zhou Xie:** Validation, Investigation. **Kai Xie:** Visualization, Data curation. **Chun-He Yang:** Writing – review & editing, Supervision.

Declaration of competing interest

The authors declare that they have no known competing financial interests or personal relationships that could have appeared to influence the work reported in this paper.

Acknowledgments

The financial support from the National Science and Technology Major Project, China (No. 2024ZD1004107) and the Natural Science Foundation of Wuhan (No. 2024040701010062) is greatly appreciated.

Appendix A. Solution for the fluid flow model

The forward difference in space and backward difference in time was used to discretize the continuity equations of free gas, dissolved gas, and crude oil. The discretization format is as follows:

$$\frac{A_{p,j}\left(E_{g,j}^{k}\rho_{g,j}^{k} - E_{g,j}^{k-1}\rho_{g,j}^{k-1}\right)}{\Delta t} \\
= \frac{A_{p,j+1}E_{g,j+1}^{k}\rho_{g,j+1}^{k}\nu_{g,j+1}^{k} - A_{p,j}E_{g,j}^{k-1}\rho_{g,j}^{k-1}\nu_{g,j}^{k-1}}{\Delta z} + m_{g,j}^{k}$$
(A.1)

$$\begin{split} &\frac{A_{\mathrm{p},j}\left(E_{\mathrm{o},j}^{k}\rho_{\mathrm{o},j}^{k}c_{\mathrm{g},j}^{k}-E_{\mathrm{o},j}^{k-1}\rho_{\mathrm{o},j}^{k-1}c_{\mathrm{g},j}^{k-1}\right)}{\Delta t} \\ &=\frac{A_{\mathrm{p},j+1}E_{\mathrm{o},j+1}^{k}\rho_{\mathrm{o},j+1}^{k}c_{\mathrm{g},j+1}^{k}\nu_{\mathrm{o},j+1}^{k}-A_{\mathrm{p},j}E_{\mathrm{o},j}^{k-1}\rho_{\mathrm{o},j}^{k-1}c_{\mathrm{g},j}^{k-1}\nu_{\mathrm{o},j}^{k-1}}{\Delta z}-m_{\mathrm{g},j}^{k} \end{split} \tag{A.2}$$

$$\frac{A_{p,j} \left(E_{o,j}^{k} \rho_{o,j}^{k} - E_{o,j}^{k-1} \rho_{o,j}^{k-1} \right)}{\Delta t} \\
= \frac{A_{p,j+1} E_{o,j+1}^{k} \rho_{o,j+1}^{k} \nu_{o,j+1}^{k} - A_{p,j} E_{o,j}^{k} \rho_{o,j}^{k} \nu_{o,j}^{k}}{\Delta z}$$
(A.3)

The drift relationship at time k is

$$v_{g,j}^{k} = C_0 \left(E_{g,j}^{k} v_{g,j}^{k} + E_{O,j}^{k} v_{O,j}^{k} \right) + v_{gr}$$
(A.4)

where C_0 is the distribution coefficient; $v_{\rm gr}$ is the drift velocity, m/s. By combining the above equations, the free gas void fraction, oil holdup, and flow velocities of free gas and oil can be obtained

$$E_{g,j}^{k} = \frac{K_{g}}{\nu_{g,j}^{k} + b_{g}}$$
 (A.5)

$$E_{0,j}^{k} = 1 - E_{g,j}^{k} \tag{A.6}$$

$$v_{0,j}^{k} = \frac{K_{0} - b_{0}E_{0,j}^{k}}{E_{0,j}^{k}}$$
(A.7)

$$v_{g,j}^{k} = C_0(K_g + K_o - b_g) + v_{gr}$$
 (A.8)

with

$$\begin{cases} K_{g} = \frac{A_{j+1}E_{g,j+1}^{k}\rho_{g,j+1}^{k}\nu_{g,j+1}^{k}}{A_{j}\rho_{g,j}^{k}} + \frac{E_{g,j}^{k-1}\rho_{g,j}^{k-1}}{\rho_{g,j}^{k}} \frac{\Delta z}{\Delta t} + \frac{\Delta h}{A_{j}\rho_{g,j}^{k}} m_{g,j}^{k} \\ K_{o} = \frac{A_{j+1}E_{o,j+1}^{k}\rho_{o,j+1}^{k}\nu_{o,j+1}^{k}}{A_{j}\rho_{o,j}^{k}} + \frac{E_{o,j}^{k-1}\rho_{o,j}^{k-1}}{\rho_{o,j}^{k}} \frac{\Delta z}{\Delta t} \end{cases}$$
(A.9)

where K_g and K_g represent the intermediate variables of gas phase and oil phase, respectively.

The flow velocity of the dissolved gas is the same as the oil phase, and the mass fraction of dissolved gas can be calculated using Eq. (A.2).

The equation for momentum conservation is employed to determine the pressure field profile, and its implicit discrete representation is

$$\begin{split} &\sum_{i=g,o} \frac{\left(A_{p}E_{i}\rho_{i}\nu_{i}\right)\big|_{j}^{k} - \left(A_{p}E_{i}\rho_{i}\nu_{i}\right)\big|_{j}^{k-1}}{\Delta t} \\ &+ \sum_{i=g,o} \frac{\left(A_{p}E_{i}\rho_{i}\nu_{i}^{2}\right)\big|_{j}^{k} - \left(A_{p}E_{i}\rho_{i}\nu_{i}^{2}\right)\big|_{j-1}^{k}}{\Delta z} \\ &+ \frac{A_{p,j}p_{p,j}^{k} - A_{p,j-1}p_{p,j-1}^{k}}{\Delta z} \\ &= -f\frac{A_{p,j}\rho_{m,j}^{k}\left(\nu_{m,j}^{k}\right)^{2}}{2d_{tin}} + A_{p,j}\rho_{m,j}^{k}g \end{split} \tag{A.10}$$

Appendix B. Solution for the heat transfer model

The discrete format of the energy conservation equation for the two-phase fluids in the central tube is

$$\begin{split} &A_{\mathbf{p},j}(\rho C)|_{\mathbf{m},j}^{k} \frac{T_{\mathbf{p},j}^{k} - T_{\mathbf{p},j}^{k-1}}{\Delta t} \\ &+ \frac{1}{2} \sum_{i=\mathbf{g},\mathbf{o}} \frac{A_{\mathbf{p},j} E_{i,j}^{k} \rho_{i,j}^{k} \left(v_{i,j}^{k}\right)^{2} - A_{\mathbf{p},j} E_{i,j}^{k-1} \rho_{i,j}^{k-1} \left(v_{i,j}^{k-1}\right)^{2}}{\Delta t} \\ &= \frac{A_{\mathbf{p},j} p_{j}^{k} - A_{\mathbf{p},j} p_{j}^{k-1}}{\Delta t} - A_{\mathbf{p},j} (\rho C v)|_{\mathbf{m},j}^{k} \frac{T_{\mathbf{p},j+1}^{k} - T_{\mathbf{p},j}^{k}}{\Delta z} \\ &- \frac{1}{2} \sum_{i=\mathbf{g},\mathbf{o}} \frac{A_{\mathbf{p},j+1} E_{i,j+1}^{k} \rho_{i,j+1}^{k} \left(v_{i,j+1}^{k}\right)^{3} - A_{\mathbf{p},j+1} E_{i,j+1}^{k} \rho_{i,j+1}^{k} \left(v_{i,j+1}^{k}\right)^{3}}{\Delta z} \\ &- A_{\mathbf{p},j} \sum_{i=\mathbf{g},\mathbf{o}} \rho_{i,j}^{k} v_{i,j}^{k} \mathbf{g} \mathbf{cos} \theta + A_{\mathbf{p},j} f_{j}^{k} \frac{\rho_{\mathbf{m},j}^{k} \left(v_{\mathbf{m},j}^{k}\right)^{3}}{2 d_{\mathbf{t}i}} + \pi d_{\mathbf{p}i} U_{\mathbf{p},j}^{k} \left(T_{\mathbf{a},j}^{k} - T_{\mathbf{p},j}^{k}\right) \end{split} \tag{B.1}$$

The discrete format of the energy conservation equation for gas in the annulus is

$$\begin{split} A_{a,j}\rho_{g,j}^{k}C_{V,g}\frac{T_{a,j}^{k}-T_{a,j}^{k-1}}{\Delta t}-A_{a,j}\left(\rho_{g,j}^{k}\mu_{JT}C_{V,g}+1\right)\frac{p_{a,j}^{k}-p_{a,j}^{k-1}}{\Delta t}\\ &+A_{a,j}\rho_{g,j}^{k}v_{a,j}^{k}\left(\frac{v_{a,j}^{k}-v_{a,j}^{k-1}}{\Delta t}+C_{V,g}\frac{T_{a,j}^{k}-T_{a,j-1}^{k}}{\Delta z}-\mu_{JT}C_{V,g}\frac{p_{a,j}^{k}-p_{a,j-1}^{k}}{\Delta z}\right)\\ &+v_{a,j}^{k}\frac{v_{a,j}^{k}-v_{a,j-1}^{k}}{\Delta z}\right)\\ &=-A_{a,j}\rho_{g,j}^{k}v_{a,j}^{k}g-\pi d_{pi}U_{p}\left(T_{a,j}^{k}-T_{p,j}^{k}\right)+\pi d_{ci}U_{a}\left(T_{e,1,j}^{k}-T_{a,j}^{k}\right) \end{split} \tag{B.2}$$

Eq. (B.2) can be further simplified as

$$\alpha T_{f,j}^{k} - \frac{\pi d_{pi} U_{p}}{A_{a}} T_{p,j}^{k} - \frac{\pi d_{ci} U_{a}}{A_{a}} T_{e,1,j}^{k} = \beta$$
(B.3)

with

$$\alpha = \frac{\rho_j^k C_{V,g}}{\Delta t} + \frac{\rho_j^k v_j^k C_{V,g}}{\Delta z} + \frac{\pi d_{pi} U_p + \pi d_{ci} U_a}{A_a}$$
(B.4)

$$\beta = \frac{\rho_{j}^{k} C_{V,g}}{\Delta t} T_{f,j}^{k-1} + \left(\rho_{j}^{k} \mu_{JT} C_{V,g} + 1 \right) \frac{p_{j}^{k} - p_{j}^{k-1}}{\Delta t} - \rho_{j}^{k} v_{j}^{k}$$

$$\left(\frac{v_{j}^{k} - v_{j}^{k-1}}{\Delta t} - C_{V,g} \frac{T_{f,j-1}^{k}}{\Delta z} - \mu_{JT} C_{V,g} \frac{p_{j}^{k} - p_{j-1}^{k}}{\Delta z} + v_{j}^{k} \frac{v_{j}^{k} - v_{j-1}^{k}}{\Delta z} \right)$$

$$- \rho_{j}^{k} v_{j}^{k} g$$
(B.5)

The discrete form of the heat transfer equation in surrounding rocks is

$$\rho_{\rm e} {\rm C_{\rm e}} \frac{T_{{\rm e},i,j}^k - T_{{\rm e},i,j}^{k-1}}{\Delta t} = \lambda_{\rm e} \left(\frac{1}{r_i} \frac{T_{{\rm e},i+1,j}^k - T_{{\rm e},i,j}^k}{r_{i+1} - r_i} + \frac{T_{{\rm e},i+1,j}^k - 2T_{{\rm e},i,j}^k + T_{{\rm e},i-1,j}^k}{(r_{i+1} - r_i)(r_i - r_{i-1})} \right) \tag{B.6}$$

By combining all the above equations and constructing a tridiagonal matrix for the solution, the temperature field distribution in the central tube, annulus, and formation can be obtained.

References

Bamidele, O.E., Hassan, M., Ahmed, W.H., 2021. Flow induced vibration of two-phase flow passing through orifices under slug pattern conditions. J. Fluid Struct. 101, 103209. https://doi.org/10.1016/j.jfluidstructs.2020.103209.

Chaves, G.S., Karami, H., Ferreira Filho, V.J.M., Vieira, B.F., 2022. A comparative study on the performance of multiphase flow models against offshore field production data. J. Petrol. Sci. Eng. 208, 109762. https://doi.org/10.1016/j. petrol.2021.109762.

Ekrann, S., Rommetveit, R., 1985. A simulator for gas kicks in oil-based drilling muds. In: SPE Annual Technical Conference and Exhibition. https://doi.org/ 10.2118/14182-MS.

Hinkebein, T.E., 2003. Compilation of gas intrusion measurements, variations, and consequence modeling for SPR caverns. Sandia National Laboratories (SNL), Albuquerque, NM, and Livermore, CA (United States). https://doi.org/10.2172/989560

Li, D., Liu, W., Jiang, D., Chen, J., Fan, J., Qiao, W., 2021. Quantitative investigation on the stability of salt cavity gas storage with multiple interlayers above the cavity roof. J. Energy Storage 44, 103298. https://doi.org/10.1016/j.est.2021.103298.

Li, W., Chen, G., Ding, S., Zhang, Y., 2022. A method for assessing the gas capacity based on thermodynamic state analysis for salt cavern during operation. J. Energy Storage 50, 104316. https://doi.org/10.1016/j.est.2022.104316.

Liao, Y., Sun, X., Sun, B., Gao, Y., Wang, Z., 2019. Transient gas-liquid-solid flow model with heat and mass transfer for hydrate reservoir drilling. Int. J. Heat Mass Tran. 141, 476–486. https://doi.org/10.1016/j.ijheatmasstransfer.2019.06.097.

Liao, Y., Zheng, J., Wang, Z., Sun, B., Sun, X., Linga, P., 2022. Modeling and characterizing the thermal and kinetic behavior of methane hydrate dissociation in sandy porous media. Appl. Energy 312, 118804. https://doi.org/10.1016/j.apenergy.2022.118804.

Liao, Y., Wang, T., Li, L., Ren, Z., Xie, D., He, T., 2023. Thermal analysis for gas storage in salt cavern based on an improved heat transfer model. Appl. Therm. Eng. 232, 121112. https://doi.org/10.1016/j.applthermaleng.2023.121112.

Liao, Y., Wang, T., Ren, Z., Wang, D., Sun, W., Sun, P., Li, J., Zou, X., 2024. Multi-well combined solution mining for salt cavern energy storages and its displacement optimization. Energy 288, 129792. https://doi.org/10.1016/j.energy.2023.129792.

Lou, W., Wang, Z., Zhang, J., Liu, H., Sun, B., Zhang, F., 2023. Flow regime evolution mechanism and falling flux prediction model for bypass injection of viscous liquid in vertical T-junction. Chem. Eng. J. 476, 146601. https://doi.org/10.1016/ i.cei.2023.146601.

Mansouri, H., Ajalloeian, R., 2018. Mechanical behavior of salt rock under uniaxial compression and creep tests. Int. J. Rock Mech. Min. Sci. 110, 19–27. https://doi.org/10.1016/j.ijrmms.2018.07.006.

Meng, Y., Xu, C., Wei, N., Li, G., Li, H., Duan, M., 2015. Numerical simulation and experiment of the annular pressure variation caused by gas kick/injection in wells. J. Nat. Gas Sci. Eng. 22, 646–655. https://doi.org/10.1016/j.ingse.2015.01.013.

Munson, D.E., 2010. Observations on vapor pressure in SPR caverns: Sources. Sandia National Laboratories (SNL), Albuquerque, NM, and Livermore, CA (United States). https://doi.org/10.2172/986599.

Nickens, H.V., 1987. A dynamic computer model of a kicking well. SPE Drill. Eng. 2, 159–173. https://doi.org/10.2118/14183-PA.

Perera, M.S.A., 2023. A review of underground hydrogen storage in depleted gas reservoirs: Insights into various rock-fluid interaction mechanisms and their

- impact on the process integrity. Fuel 334, 126677. https://doi.org/10.1016/j.
- Rommetveit, R., Blyberg, A., Olsen, T.L., 1989. The effects of operating conditions, reservoir characteristics and control methods on gas kicks in oil based drilling muds. In: SPE Offshore Europe. https://doi.org/10.2118/19246-MS.
- Ruckenstein, E., Davis, E.J., 1970. Diffusion-controlled growth or collapse of moving and stationary fluid spheres. J. Colloid Interface Sci. 34, 142–158. https://doi. org/10.1016/0021-9797(70)90267-5.
- Sun, B., Sun, X., Wang, Z., Chen, Y., 2017. Effects of phase transition on gas kick migration in deepwater horizontal drilling. J. Nat. Gas Sci. Eng. 46, 710–729. https://doi.org/10.1016/j.ingse.2017.09.001.
- Sun, B., Fu, W., Wang, N., Wang, Z., Gao, Y., 2019. Multiphase flow modeling of gas intrusion in oil-based drilling mud. J. Petrol. Sci. Eng. 174, 1142–1151. https://doi.org/10.1016/j.petrol.2018.12.018.
- Tackie-Otoo, B.N., Haq, M.B., 2024. A comprehensive review on geo-storage of H₂ in salt caverns: Prospect and research advances. Fuel 356, 129609. https://doi.org/10.1016/j.fuel.2023.129609.
- Tarkowski, R., 2019. Underground hydrogen storage: Characteristics and prospects. Renew. Sustain. Energy Rev. 105, 86–94. https://doi.org/10.1016/j.rser.2019.01.051.
- Wang, N., Sun, B., Wang, Z., Wang, J., Yang, C., 2016. Numerical simulation of two phase flow in wellbores by means of drift flux model and pressure based method. J. Nat. Gas Sci. Eng. 36, 811–823. https://doi.org/10.1016/j.jngse.2016.10.040.
- Wang, T., Liao, Y., He, T., Xie, D., Ren, Z., Qin, K., Zhang, C., 2025. Oil recovery and cooling for underground salt cavern oil storage: Insights from coupled flow and thermal model. Geoenergy Sci. Eng. 244, 213456. https://doi.org/10.1016/j.geoen.2024.213456.
- Wang, Z., Sun, B., Wang, J., Hou, L., 2014. Experimental study on the friction coefficient of supercritical carbon dioxide in pipes. Int. J. Greenh. Gas Control 25, 151–161. https://doi.org/10.1016/j.ijggc.2014.04.014.
- Wang, Z., Liu, J., Zhong, S., Qiao, L., Li, W., Guo, J., 2023. Hydrogeological model for underground oil storage in rock caverns. Tunn. Undergr. Space Technol. 132, 104880. https://doi.org/10.1016/j.tust.2022.104880.

- Wei, X., Shi, X., Li, Y., Li, P., Ban, S., Zhao, K., Ma, H., Liu, H., Yang, C., 2023. A comprehensive feasibility evaluation of salt cavern oil energy storage system in China. Appl. Energy 351, 121807. https://doi.org/10.1016/j.apenergy.2023.121807.
- Wei, X., Shi, X., Ma, H., Ban, S., Bai, W., 2024. Experimental investigation on the oil extraction process for a novel underground oil storage method: Oil storage in salt cavern insoluble sediment voids. Energy 309, 133061. https://doi.org/ 10.1016/j.energy.2024.133061.
- Williams, J.D.O., Williamson, J.P., Parkes, D., Evans, D.J., Kirk, K.L., Sunny, N., Hough, E., Vosper, H., Akhurst, M.C., 2022. Does the United Kingdom have sufficient geological storage capacity to support a hydrogen economy? Estimating the salt cavern storage potential of bedded halite formations. J. Energy Storage 53, 105109. https://doi.org/10.1016/j.est.2022.105109.
- Xi, X., Zhou, J., Gao, X., Liu, D., Zheng, H., Sun, Q., 2019. Impact of changes in crude oil trade network patterns on national economy. Energy Econ. 84, 104490. https://doi.org/10.1016/j.eneco.2019.104490.
- Xie, D., Wang, T., Li, L., Guo, K., Ben, J., Wang, D., Chai, G., 2023. Modeling debrining of an energy storage salt cavern considering the effects of temperature. Energy 282, 128845. https://doi.org/10.1016/j.energy.2023.128845.
- Xu, C., Gao, Y., Qin, Z., Li, Z., Pan, S., Qi, L., 2024. Historical characteristics and projection of global renewable energy consumption. Renew. Energy 234, 121222. https://doi.org/10.1016/j.renene.2024.121222.
- Yang, C., Wang, T., Li, Y., Yang, H., Li, J., Qu, D., Xu, B., Yang, Y., Daemen, J.J.K., 2015. Feasibility analysis of using abandoned salt caverns for large-scale underground energy storage in China. Appl. Energy 137, 467–481. https://doi.org/10.1016/j.apenergy.2014.07.048.
- Zhang, N., Shi, X., Wang, T., Yang, C., Liu, W., Ma, H., Daemen, J.J.K., 2017. Stability and availability evaluation of underground strategic petroleum reserve (SPR) caverns in bedded rock salt of Jintan, China. Energy 134, 504–514. https://doi. org/10.1016/j.energy.2017.06.073.